ARTICLES
https://doi.org/10.1038/s41560-019-0427-x
nature energy

# High-capacity methane storage in flexible alkane-linked porous aromatic network polymers

Vepa Rozyyev[1], Damien Thirion[1], Ruh Ullah[2], Joosung Lee[1], Minji Jung[3], Hyunchul Oh[3], Mert Atilhan[4,5]* and Cafer T. Yavuz[1,6,7]*

**Adsorbed natural gas (ANG) technology is a viable alternative to conventional liquefied or compressed natural-gas storage. Many different porous materials have been considered for adsorptive, reversible methane storage, but fall short of the US Department of Energy targets (0.5 g g$^{-1}$, 263 l l$^{-1}$). Here, we prepare a flexible porous polymer, made from benzene and 1,2-dichloroethane in kilogram batches, that has a high methane working capacity of 0.625 g g$^{-1}$ and 294 l l$^{-1}$ when cycled between 5 and 100 bar pressure. We suggest that the flexibility provides rapid desorption and thermal management, while the hydrophobicity and the nature of the covalently bonded framework allow the material to tolerate harsh conditions. The polymer also shows an adsorbate memory effect, where a less adsorptive gas ($N_2$) follows the isotherm profile of a high-capacity adsorbate ($CO_2$), which is attributed to the thermal expansion caused by the adsorption enthalpy. The high methane capacity and memory effect make flexible porous polymers promising candidates for ANG technology.**

The design principles for adsorbed natural gas (ANG) sorbents were always thought to require rigid building blocks to provide high specific surface areas[1–4]. These yielded many framework structures with remarkably large contact surfaces[5–7]. However, because the pores were permanently locked, complete pore filling always took place in relatively low-pressure regimes (for example <10 bar), and increasing pressure had little effect on the adsorption capacity after reaching saturation[2,3]. In contrast, ANG design necessitates a higher-pressure window (5 to 50–250 bar), rendering highly sorptive porous media with Langmuir-type adsorptive behaviour less effective[2,8]. Recently, flexible linkers were used in an otherwise rigid porous metal–organic framework (MOF) to reach high usable capacities in methane uptake[2]. The highly recyclable gate opening behaviour provided substantial methane uptake capacities (0.204 g g$^{-1}$ and 197 l l$^{-1}$), despite still being short of the targets set by the US Department of Energy (DOE), 0.5 g g$^{-1}$ and 263 l l$^{-1}$. One recent, remarkable example of such flexible mechanisms is negative gas adsorptions by DUT-49, where pores contract with the increased pressure, providing upward profiles of hysteretic gas storage[8]. In addition to the below-target working capacities, the low mechanical endurance of most MOFs would prove unattractive during compression–decompression cycles as well as pellet making[9].

In this paper, we turned to flexible, carbon–carbon bonded, porous, network polymers to build a porous material that would employ a similar flexible mechanism and use the adsorption enthalpy for framework expansion, but be very stable against mechanical impact and impurities such as water, hydrogen sulfide and higher hydrocarbons, as well as being scalable and affordable. In doing so, we synthesized 29 porous polymeric structures with inherent flexibility and achieved a high deliverable methane working capacity of 0.625 g g$^{-1}$ and 294 l l$^{-1}$ when cycled between 5 and 100 bar. During cyclic tests of $CO_2$ and $N_2$ uptake we observed an adsorbate memory effect, a promising feature for long-term gas storage.

## Design of a flexible porous polymer for methane storage

It is known that adsorptive enhancement is best practised by incorporating target-specific functional groups inside a superstructure[10,11]. For methane storage, open metal sites (HKUST-1)[3,12], trifluoromethyl[13], pyrimidine[14] and aromatic (PCN-14)[15] rings such as anthracene and ethylene[16] have been shown to be effective. Methanophilic ethylene groups are particularly interesting, as they enhance the total methane uptake of materials and their aliphatic nature could bring the much needed flexibility for high working capacity. Conceptually, we arrived at the union of an aromatic core to provide a basis for the framework structure and ethylene extensions for flexible linkers to expand the pore shaped by the aromatic blocks. Our investigation of synthetic methodologies led to the Friedel–Crafts alkylation, an industrially well established reaction for rapid formation of alkylated aromatics[17]. We have chosen an array of cores and linkers that would lead to 29 unique porous polymers, with varying synthetic complexities, porosities and morphologies (see Supplementary Notes 1 and 2 for details).

In Friedel–Crafts reactions that form polymers, it is common to use a solvent that mixes well with the reactants and the catalyst[18–20]. Often it is a chlorinated alkane, despite the possible unwanted chemical reaction between the Lewis acid and the alkyl chloride solvent. We set out to exploit precisely this possibility and found that the solvent could also easily act as a linker, producing a robust three-dimensional network polymer with excellent atom economy. The only critical concern was overalkylation, which would secede the framework extension. On the contrary, we predicted that the intermediates would be more reactive than the starting material. Hence, the extended framework was kinetically trapped (Fig. 1). In a reaction of benzene and 1,2-dichloroethane (DCE, as both solvent and linker), we successfully produced a highly reproducible, carbon–carbon bonded network polymer (indexed henceforth as covalent organic polymer,

[1]Graduate School of EEWS, Korea Advanced Institute of Science and Technology (KAIST), Daejeon, Korea. [2]National Institute for Materials Science (NIMS), Tsukuba, Japan. [3]Department of Energy Engineering, Gyeongnam National University of Science and Technology (GNTECH), Jinju, Korea. [4]Department of Chemical Engineering, Texas A&M University at Qatar, Doha, Qatar. [5]Gas and Fuels Research Center, Texas A&M University, College Station, TX, USA. [6]Department of Chemical and Biomolecular Engineering, KAIST, Daejeon, Korea. [7]Department of Chemistry, KAIST, Daejeon, Korea. *e-mail: mert.atilhan@qatar.tamu.edu; yavuz@kaist.ac.kr

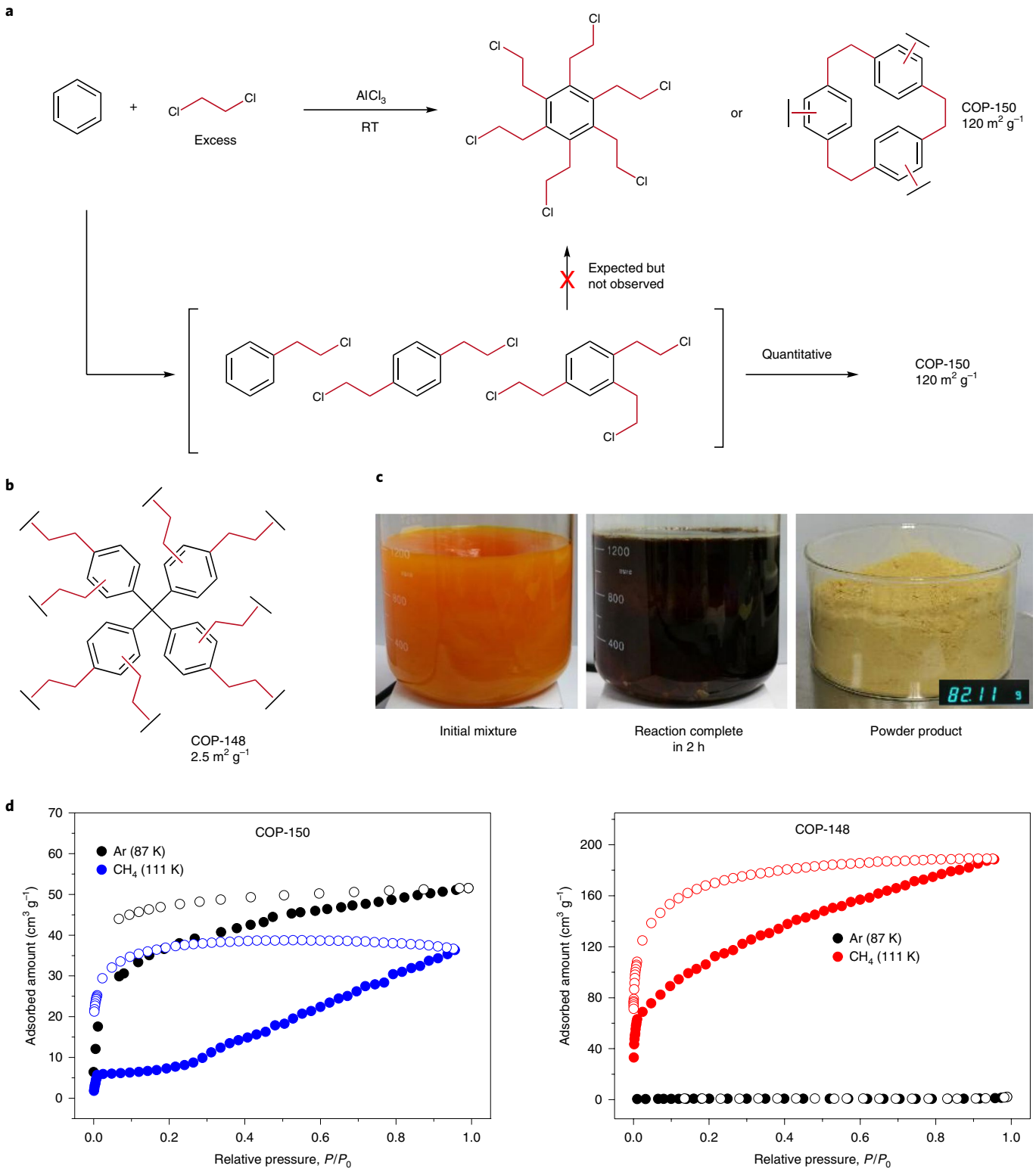


**Fig. 1 | Design and synthesis of flexible porous polymers. a**, Synthesis of COP-150 by kinetically trapping highly reactive intermediates. In conventional Friedel–Crafts reactions, overalkylation is expected when excess alkyl chloride is used. However, because the alkylated benzenes have higher reactivity than the alkyl chloride, the porous network structures form quantitatively. **b**, COP-148 was synthesized similarly starting from tetraphenylmethane. **c**, Photographs of the COP-150 synthesis at small scale (82.11 g of product). Note that the reaction is carried out in a beaker open to the air. **d**, Ar (87 K) and methane (111 K) isotherms for COP-150 and COP-148. Filled symbols denote adsorption and open symbols refer to desorption.

COP-150) with high ultramicroporosity and modest specific surface areas in the ground state (120 $m^2 g^{-1}$ from Ar adsorption at 87 K for 5 d of measurement). A close procedure was recently reported, although the reaction of $AlCl_3$ with DCE at 80 °C also leads to self-polymerization of DCE (without benzene) and possibly carbonization[21].

COP-150 features two key chemical components for methanophilic behaviour: aromatic rings and an aliphatic, hydrophobic hydrocarbon framework. In addition, its ethylene bridges would allow rotational freedom and wide-angle bending, enabling structural expansion with external stimuli. We therefore screened DCE, dichloromethane and chloroform reactions of the commercial aromatic hydrocarbons to produce 29 new structures (COPs 124–152). It is important to note that our synthetic methodology also sheds light on previous claims of Scholl-type aromatic couplings taking place in similar settings[22,23], as our data suggest that alkyl bridging reactions are more feasible than the aryl couplings if chlorinated alkanes are used as solvents (see Supplementary Note 3 and Supplementary methods for detailed methods and evaluations).

## High-pressure reversible methane storage

In the performance evaluation of the adsorbents for the ANG systems, instead of total adsorption capacity, working capacity[24] (also defined as deliverable or usable capacity) is crucial (Fig. 2). A minimum inlet pressure of about 5 bar is required to push the gas to the engine, making adsorbed capacity below 5 bar not usable. The temperature of the operation has a direct impact on the working capacity, although lowering the temperature increases low-pressure (<5 bar) capacity as well, leading to no tangible gains for most highly porous materials.

To study the ANG performances, we subjected 0.2–0.5 g of each porous polymer to pure methane gas under various conditions (Fig. 2). At 273, 278 and 283 K, methane adsorption isotherms of COP-150 show two-step adsorption. Above a certain pressure for each temperature (48 bar in the case of 273 K), methane uptake starts to increase steeply up to 100 bar without reaching saturation (Fig. 2). We believe that the increased pressure flexes the network structure of COP-150 to show swelling behaviour (also known as breathing)[25].

The pressure-triggered flexible structure of COP-150 is advantageous in terms of the total working capacity of deliverable methane in real applications. Indeed, at 273 K, COP-150 showed a gravimetric working capacity (5–100 bar) of 0.625 g g$^{-1}$, which is 98% of the total uptake capacity (0.640 g g$^{-1}$). To the best of our knowledge, this value is the highest reported gravimetric working capacity of any porous material reported, and it is 25% above the US DOE target[3,4]. On the basis of a bulk tap density of 0.34 g ml$^{-1}$, COP-150 showed a volumetric working capacity (5–100 bar) of 294 cm$^3$ cm$^{-3}$, which is also, to the best of our knowledge, the highest reported volumetric working capacity, and is 12% higher than the US DOE target.

In the case of COP-148, the structure is also flexible and ethylene linked, but synthesized from a more rigid tetraphenylmethane and DCE (Fig. 1). Similarly to COP-150, the framework density of COP-148 (1.26 g ml$^{-1}$) is lower than that of other carbon-based materials, indicating inaccessible pores at low pressures. Therefore, we believe that the flexible structure of COP-148 opens up to become highly porous: inaccessible pores become available for adsorption and the structure expands to create new pores. At 273 K, COP-148 showed a gravimetric working capacity (5–80 bar) of 0.762 g g$^{-1}$, which is 96% of the total capacity (0.790 g g$^{-1}$). Despite being a non-porous structure, it has even higher capacity than COP-150, 52% higher than the US DOE target. COP-148 also showed a very low bulk tap density of 0.076 g ml$^{-1}$. Because of its low packing density, its volumetric working capacity could only reach 81 cm$^3$ cm$^{-3}$. Despite the high gravimetric uptake, the low volumetric capacity and the cost of the tetraphenylmethane may make COP-148 less commercially viable.

For the structural contribution to the uptake capacity that is devoid of interstitial pores, the framework (true) density of COP-150 was measured to be 1.216 g ml$^{-1}$ from He free-space measurements[26]. This value is much lower than those of other carbon-based materials, such as 2.260 g ml$^{-1}$ for graphite, 2.100 g ml$^{-1}$ for PPN-4 and 2.42 g ml$^{-1}$ for AX-21 (refs. [1,26–28]), indicating that COP-150 contains pores that are not accessible at lower pressures. At higher pressures, through expansion, these pores become available for adsorption (also known as gate opening).

## Methane storage testing in a commercial cylinder

To provide more realistic data on the ANG performance, we placed 30 g of yellow COP-150 powder in a 142 ml stainless steel Swagelok cylinder and filled it with methane up to 100 bar at 20 °C (Table 1). When compared with the empty cylinder capacity under the same conditions with corrected free-space volume, a 0.219 g g$^{-1}$ uptake was observed. It is important to note that these conditions reflect the actual field operations without any control on the cylinder (for example no vacuum treatment, sample drying or processing), and could safely give the expected operational capacity in a vehicular setting. Also, it is known that when real packing densities are used the uptake capacities of literature materials typically decrease to 60% of laboratory measurements[2]. To the best of our knowledge, no literature reports these conditions for any of the highest-performing materials; perhaps the scalability and moisture sensitivity are the chief factors.

For industrial-scale natural-gas storage, the economic feasibility of the adsorbents is an important factor. Unfortunately, most of the best-performing materials require a lengthy multistep synthesis of organic linkers, often with no proven scale-up procedures. Because of our sustainable approach of using widely available substrates and catalysts, all 29 COPs synthesized in this study are reasonably affordable (especially when compared with literature examples) and readily scalable. In particular, the best-performing structure, COP-150, is made from the cheapest building blocks of all 29, roughly US$1 kg$^{-1}$ on the basis of the chemicals, and should become cheaper with mass production. Moreover, the synthesis takes place at room temperature, open to the air, and no previous purification of the chemicals is required (Fig. 1).

As a control for the flexible adsorptive mechanism, we selected polystyrene, as it would reflect the impact of chain mobility and plasticization, while being closely related in chemical composition, that is benzenes linked by aliphatic chains. However, in both Swagelok (Table 1) and high-pressure PCTPro measurements (Supplementary Fig. 7), we found that polystyrene does not follow the flexible behaviour that is displayed by COP-150 and COP-148. Studying wide-angle X-ray scattering profiles (Supplementary Fig. 31) also yielded no crystallization under high pressure, and differential scanning calorimetry readings indicated a plasticization-free nature. Flexibility was further tested by non-polar solvent uptake measurements of the network polymers (Supplementary Fig. 32). COP-148 showed the highest uptake of all three solvents tested: hexane, methanol and chloroform. COP-150 and other control structures showed less uptake, following the trend of gravimetric uptake in high-pressure methane capacity measurements, confirming the gas-induced flexibility by liquid probes.

## Observation of an adsorbate memory effect

To exploit the highly flexible nature of COP-150, we looked into high-pressure $CO_2$ and $N_2$ gas adsorptions. The high-pressure $N_2$ adsorption isotherm of COP-150 showed flat physisorptive adsorption with low uptake capacity, as expected (Fig. 3). Under high pressure (up to 200 bar) of $CO_2$, however, there is strong hysteresis with higher capacity, indicating swelling behaviour. Hysteresis is more pronounced at low temperatures, indicating more flexibility. An unusual behaviour was then observed when $N_2$ was tested immediately after a $CO_2$ adsorption cycle and vacuum treatment. The high-pressure $N_2$ adsorption isotherm showed hysteretic behaviour with higher uptake capacity, just as in the $CO_2$ adsorption isotherm (Fig. 3). Interestingly, a subsequent $N_2$ adsorption cycle on the same sample showed flat physisorptive adsorption with lower uptake capacity, just as in the original $N_2$ adsorption (of the fresh sample). After repeated measurements and recalibrating our equipment for potential errors, we confirmed an 'adsorbate

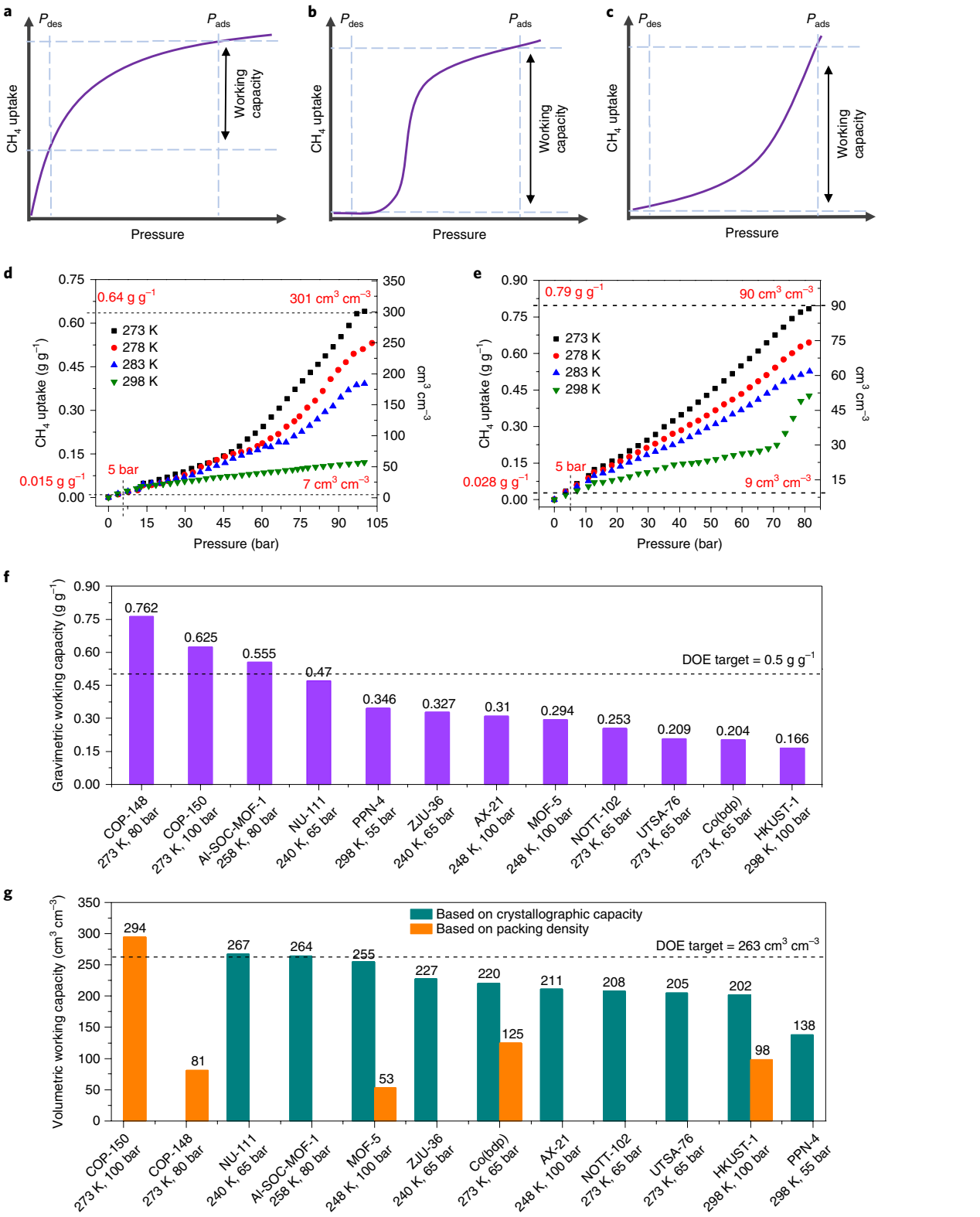


**Fig. 2 | Reversible methane uptake by flexible porous polymers. a–c**, Methane adsorption isotherm profiles of conventional, rigid, porous materials (**a**), flexible MOFs (for example Co(bdp), ref. [2]) (**b**) and flexible porous polymers (**c**). $P_{ads}$ represent the pressure at which adsorption is carried out. $P_{des}$, similarly, reflects the desorption pressure. **d**, Methane adsorption isotherms of COP-150 at four different temperatures (desorption isotherms follow same trend and were omitted for clarity); **e**, methane adsorption isotherms of COP-148 at four different temperatures; **f**, comparison of some of the highest reported gravimetric working capacities (5 bar—$P_2$) in the literature[2,3,26,27,31–33]; **g**, comparison of highest reported volumetric working capacities (5 bar—$P_2$)[2,3,26,27,31,33]. See Methods, Supplementary methods and Supplementary Figs. 3–8 for details of measurements and calculations.

**Table 1 | Real-life large-scale methane storage by COP-150 and control materials in a Swagelok cylinder**

| Adsorbent[a] | $S_{BET}$[b] ($m^2\,g^{-1}$) | $V_p$[c] ($ml\,g^{-1}$) | $\rho_{pack}$[d] ($g\,ml^{-1}$) | $\rho_{frw}$[e] ($g\,ml^{-1}$) | Cost[f] (US$\,kg^{-1}$) | Cycle | Excess uptake[g] ($g\,g^{-1}$) | | Storage capacity[h] ($g\,g^{-1}$) | |
|---|---|---|---|---|---|---|---|---|---|---|
| | | | | | | | 65–5 bar | 100–5 bar | 65–5 bar | 100–5 bar |
| COP-150 | 120 | 0.062 | 0.34 | 1.22 | 1.1 | 1st | 0.033 | 0.067 | 0.137 | 0.219 |
| | | | | | | 5th | 0.033 | 0.059 | 0.137 | 0.211 |
| | | | | | | 15th | 0.032 | 0.060 | 0.136 | 0.215 |
| HKUST-1 | 1,785 | 0.698 | 0.41 | 2.70 | 84.2 | 1st | 0.018 | 0.051 | 0.110 | 0.184 |
| | | | | | | 5th | 0.011 | 0.035 | 0.103 | 0.170 |
| | | | | | | 15th | 0.017 | 0.042 | 0.109 | 0.177 |
| Polystyrene (350,000 g mol−1) | Non-porous | — | 1.05 | 1.21 | 50.7 | 1st | 0.006 | 0.012 | 0.008 | 0.013 |
| | | | | | | 2nd | 0.006 | 0.011 | 0.008 | 0.013 |
| | | | | | | 3rd | 0.007 | 0.012 | 0.008 | 0.014 |

[a]For each measurement 30 g ($m_{ads}$) of adsorbent was used. [b]Brunauer–Emmett–Teller surface area was obtained from the 87 K Ar adsorption isotherms. [c]Total pore volume was obtained from the 87 K Ar adsorption isotherm at $P/P_0 = 0.99$. [d]Packing density ($\rho_{pack}$) was measured after 100 tappings, with a ±7% error. [e]Framework density ($\rho_{frw}$) was calculated from He free-space measurements at 298 K, 0.5 bar, and as an average of 20 measurements with a ±2.5% error. [f]COP-150 cost was calculated from wholesale prices of monomers (assuming that solvent and catalyst could be recovered); HKUST-1 price was obtained from ref. [34]; polystyrene was purchased from Sigma Aldrich (1 kg scale). [g]Excess uptakes ($q_{exc}$) were calculated using measured framework densities of the materials with the equation $q_{exc} = (m_{CH_4\,(ads)} - m_{CH_4\,(empty)} + \rho_{CH_4} m_{ads}/\rho_{frw})/m_{ads}$; uptake capacities were measured with a ±5% error. [h]Storage capacities ($q_{str}$) were calculated using packing densities of the materials with the equation $q_{str} = (m_{CH_4\,(ads)} - m_{CH_4\,(empty)} + \rho_{CH_4} m_{ads}/\rho_{pack})/m_{ads}$; uptake capacities were measured with a ±5% accuracy.

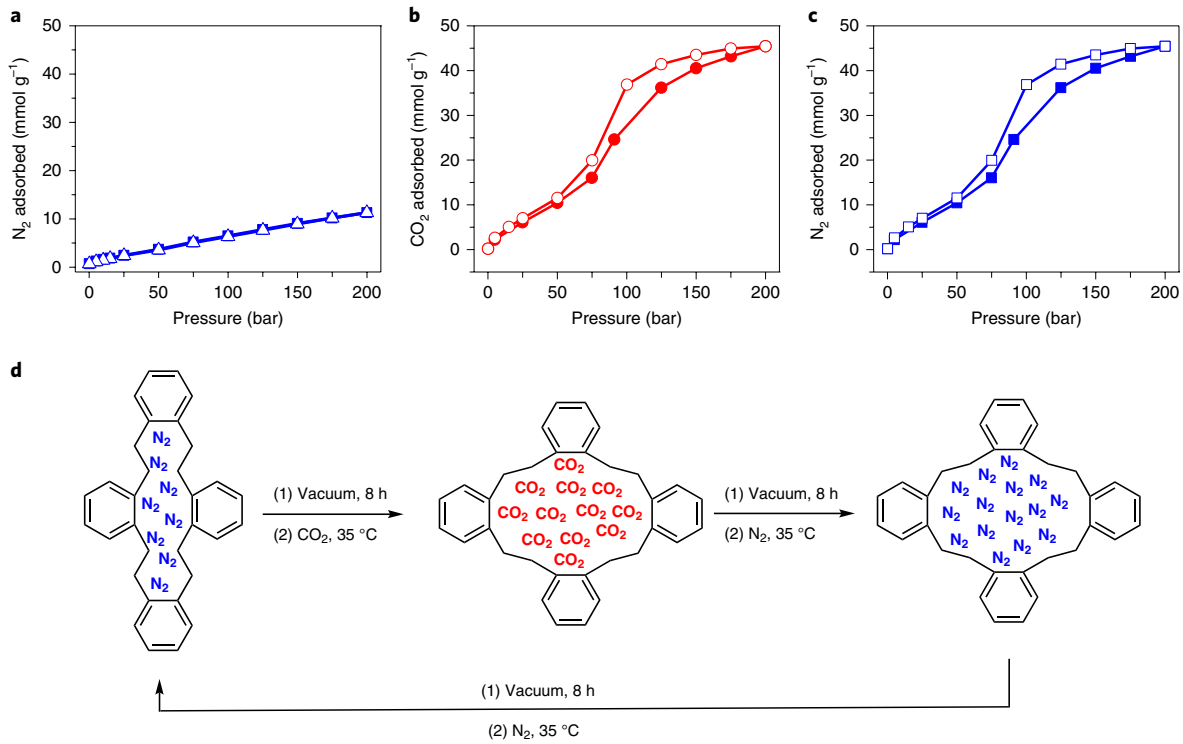


**Fig. 3 | Adsorbate memory effect. a**, $N_2$ adsorption up to 200 bar (35 °C) with a fresh sample of COP-150. **b**, $CO_2$ uptake of COP-150 up to 200 bar (35 °C). **c**, $N_2$ adsorption immediately after the $CO_2$ uptake experiment. The samples were stored under vacuum for 8 h in between gas doses. **d**, A schematic illustration of the proposed adsorbate memory effect.

memory effect' (Methods and Supplementary methods). In this, we believe, $CO_2$ expands the network structure during adsorption and the stabilized expanded structure remains intact at desorption. When $N_2$ is introduced into the swollen structure (even after 8 h of vacuum), it shows a $CO_2$-like adsorption isotherm. Since $N_2$ cannot provide the adsorbate memory recorded for $CO_2$, the structure returns to the ground state on desorbing $N_2$. A subsequent $N_2$ adsorption isotherm, then, is the same as the original, expected adsorption profile. We observed the same adsorbate memory effect in other COPs, such as COP-147 and COP-152 (Supplementary Figs. 19 and 20). The origins of this observation need more in-depth analysis and should be studied further in the future. One possibility is that adsorbate-induced surface reconstruction behaviour may arise from the changes in free energy as a function of

the surface configuration, which is determined by the adsorbate coverage with different gases. At a critical value of this coverage, the surface adopts a further stable equilibrium conformation, as observed in the case of $CO_2$. This was possible only with flexible porous polymer. Another plausible mechanism would be foam formations under high-pressure $CO_2$. On desorption, the structure does not immediately relax, but a new adsorbate with adsorptive energy input would readily influence defoaming. More in-depth studies are needed to confirm this mechanism or others.

## Conclusions

In this work, we designed flexible porous polymers based on strong carbon–carbon bonds and tested their methane gas uptake under high pressures. Of 29 distinct structures, COP-150 has shown a 0.625 g g$^{-1}$ (294 l l$^{-1}$) working capacity, surpassing the US DOE target of 0.5 g g$^{-1}$ (263 l l$^{-1}$). Higher capacities were also measured in a commercial cylinder setting for COP-150 than for any of the controls we tested, such as HKUST-1 and polystyrene. During high-pressure tests of $CO_2$ and $N_2$, COP-150 showed a memory effect based on the previous adsorbate. Together with high methane uptake capacity, this adsorbate memory effect reveals a strong promise for an enhanced gas storage procedure when flexible sorbents are employed. In the future, one potential direction could be to install more methanophilic functional groups in flexible porous polymers, such as perfluorinated alkanes or phenazines, to maximize methane storage capacities.

## Methods

**Materials.** Dichloromethane (99.5%), chloroform (99.5%), DCE (99.0%), benzene (99.5%), toluene (99.7%), xylene (99.5%), 1,2-dichlorobenzene (99.0%), pyridine (99.0%), phenol (99.0%), aniline (99.0%), naphthalene (99.0%), anhydrous iron(III) chloride (98%) and methanol (99.0%) were purchased from Samchun Pure Chemicals. Diphenyl ether (99.0%), diphenylamine (99.0%), triphenylamine (98%), triphenylphosphine (99.0%), HKUST-1 (Basolite C300, produced by BASF), polystyrene (350,000 g mol$^{-1}$) and deuterated chloroform (99.96% deuterium and contains tetramethylsilane) were purchased from Sigma Aldrich. Triphenylmethane, tetraphenylmethane (98%) and 1,3,5-triphenylbenzene (99%) were purchased from Alfa Aesar. Mesitylene (97%) and biphenyl (99%) were purchased from Acros Organics. 1-Bromoadamantane and 2-bromo-2-methylpropane were purchased from Tokyo Chemical Industry. Aluminium chloride (95%) and phosphorus pentoxide were purchased from Junsei Chemicals. Dichloromethane, chloroform and DCE were distilled over phosphorus pentoxide under a $N_2$ atmosphere (when they are referred to as dry solvents). All the other solvents were used without further purification for washing purposes or as Soxhlet extraction solvents (see Supplementary Table 1 for physical properties and hazard information for the chemicals used).

**General experimental procedure for the alkane-linked COPs.** In a 30 ml glass vial, aromatic hydrocarbon (mostly solid) is sealed with a rubber septum along with dry solid $AlCl_3$ and a stir bar. The vial is flushed thoroughly with $N_2$ gas to maintain an inert atmosphere. An excess amount of the linker solvent is injected into the vial and the mixture is stirred for 48 h under a blanket of $N_2$ atmosphere (caution: HCl might build up the pressure in the vial). After 48 h, the reaction is quenched by slow addition of methanol (caution: the $AlCl_3$–methanol reaction is highly exothermic). The precipitates are filtered and washed with methanol and chloroform (10 ml each). To remove contamination, solids are washed in a Soxhlet extractor with a 100 ml chloroform and 100 ml methanol mixture for 24 h. The products are dried at 120 °C under vacuum for 12 h.

**Large-scale synthesis of COP-150.** In a 2 l beaker, a solution of 50 ml benzene in 1 l of DCE was added to 150 g of anhydrous $AlCl_3$ and the mixture was stirred at room temperature open to the air. After about 40 min, stirring was no longer possible because of the aggregates around the stirring bar (caution: HCl gas evolution; conduct experiment inside a proper fume hood). After 18 h, the reaction mixture was slowly quenched by adding a methanol ice mixture (1 l) and mechanically breaking the chunks of aggregates (caution: the $AlCl_3$–methanol/water reaction is highly exothermic; add solvent slowly). After quenching, solids were filtered, dried and ground into fine powder. The powder was washed twice with 1.0 l of water with stirring for 4 h at 80 °C, four times with 1.0 l of ethanol with stirring for 6 h at 60 °C, twice with 1.0 l of chloroform with stirring for 6 h at 60 °C and finally twice with 1.0 l of dichloromethane with stirring for 6 h at room temperature. The product was dried under vacuum at 100 °C. 82 g of yellow powder was obtained.

**Synthesis of COP-148.** Tetraphenylmethane (0.50 g), $AlCl_3$ (0.84 g) and a stirring bar were placed in a 30 ml glass vial closed tightly with a rubber septum. The vial was flushed with $N_2$ gas and injected with 10 ml of dry DCE before stirring for 48 h under a $N_2$ atmosphere (caution: HCl might build up the pressure in the vial). The reaction was quenched slowly by adding methanol (caution: the $AlCl_3$–methanol reaction is highly exothermic). The precipitate was filtered and washed with methanol and chloroform (10 ml each), and then in a Soxhlet extractor with a 100 ml chloroform and 100 ml methanol mixture for 24 h. After washing, the product was dried at 100 °C under vacuum for 12 h.

**Characterization.** Elemental analyses were performed at the KAIST Central Research Instrument Facility on a Thermo Scientific FLASH 2000 series (CHNS) analyser equipped with a thermal conductivity detector. The instrument has a detection range of 0.01%–100% composition within 15 min for a sample size of 0.1–100 mg, and measures the elemental composition of the materials with an accuracy of 0.3%. All the measurements were made using samples of 1.5–2 mg per measurement, and reported elemental compositions are averages of two different measurements of the same sample. Residual aluminium content in COPs was determined by inductively coupled plasma measurement on an Agilent 7700s ICP-MS. Solid-state $^{13}C$ cross-polarization magic angle spinning NMR was performed at the KAIST Central Research Instrument Facility on a Bruker Avance III 400 WB NMR spectrometer, 400 MHz 54 mm DD2 equipped with a high frequency (HFXY) 1.6 mm probe. The contact time was 5 ms with a delay of 3 s. All samples were spun at 5 kHz. All the powder samples (weights about 200–300 mg) were ground well and ensured to be dry before analyses. Fourier transform attenuated total reflectance infrared spectra were recorded with a Shimadzu IRTracer, GladiATR 10 Fourier transform infrared spectrometer. A properly dried sample (2 mg) was placed beneath the tip of the laser and scanned 20 times. The background data were deleted from the sample data; the baseline was corrected and the data were smoothed before recovery. Thermogravimetric analyses were performed on a Shimadzu DTG-60A by heating the samples from 30 °C to 800 °C at a rate of 10 °C min$^{-1}$ under a $N_2$ atmosphere. Alumina pans were used for both sample and reference scans over the magnetic balances. Scanning electron microscopy images were taken using an FEI Magellan400 field emission scanning electron microscope. Samples were prepared by coating with a Vacuum Device HPC-1SW osmium coater on a carbon tape pasted on a flat circular (aluminium) holder under a pressure of 0.06 mbar for 15 min before imaging. Freeze-drying measurements were made in an ilShin Biobase lyophilizer at about −50 °C for 18 h.

**Porosity and low-pressure gas adsorption–desorption properties.** The porosities of the polymers were analysed from argon adsorption–desorption isotherms using a Micromeritics 3FLEX accelerated surface area and porosimetry analyser at 87 K. Before measurement, samples were degassed at 423 K for 6 h under vacuum. The specific surface areas were derived using the Brunauer–Emmett–Teller method. All pore size distributions were calculated with the Micromeritics 3FLEX software using a non-local density functional theory model with slit pores[29] (see Supplementary Note 2 and Supplementary Table 9 for more details of porosity analysis and low-pressure gas adsorption study).

**High-pressure methane uptake experiments.** Samples were measured in the range of 0–100 bar on a Pressure–Concentration/Composition–Temperature Pro (PCTPro) instrument. The PCTPro is a fully automated Sievert instrument for the measurement of gas sorption properties of different materials. The PCTPro is able to determine the gas sorption properties of both solids and liquids at various temperatures and pressures on the basis of the volumetric measurement method. A sample at known pressure and volume is subjected to a reservoir of known volume (0 ml, 17 ml, 24 ml, 75 ml, 124 ml) and pressure (0–400 bar) through an isolation valve (Supplementary Fig. 3). On opening the isolation valve, a new equilibrium is established since some gas is absorbed/adsorbed by the sorbent, and the gas sorption quantity is determined by the difference in actual measured pressure ($P_f$) versus calculated pressure ($P_c$). The pressure–composition isotherm is produced in the form of a curve from the concentration of gas sorbed and the final pressure of each dose in a series of many doses that either increase (absorption) or decrease (desorption) in pressure. All isothermal measurements were made at single fixed temperature, while the gas was applied and removed through small and well defined doses with each aliquot reaching the equilibrium state. The equilibrium state was jointly defined by the gas pressure and temperature[30].

Total methane adsorption capacities of the studied materials were calculated from excess capacities using an equation of total uptake = excess uptake + (pore volume × density of methane). NIST RefProp and Roland Span's reference equations of state were used for the calculation of methane densities at respective temperatures and pressures (see Supplementary Methods and Supplementary Figs. 3–8 for more details of high-pressure methane adsorption measurements).

**Large-scale, real-life methane storage experiments.** All large-scale methane uptake measurements were conducted using a Swagelok sample cylinder at the World Gas company located in Daejeon, South Korea (caution: pure methane gas under pressure must be handled in safety-certified environments). The available volume of the cylinder for the methane gas is 142.5 ml. Each experiment contained

three steps: (1) measuring the mass of an empty (without gas) cylinder, (2) filling with gas to the desired pressure and waiting for stabilization of the pressure for at least 30 min and (3) measuring the mass of the cylinder containing high-pressure methane. All experiments were conducted in a room at a temperature of 30(±2) °C (see Supplementary methods and Supplementary Figs. 9 and 10 for more details of large-scale methane storage experiments).

**Adsorbate memory effect.** High-pressure $N_2$ and $CO_2$ sorption experiments were carried out in the range of 0–200 bar on a Rubotherm magnetic suspension sorption apparatus based on magnetic levitation. Measurements start with placing an approximately 0.25 g of a sorbent sample in the sample holder after activation by degassing at 150 °C. Once the sample is in place, the system is placed under vacuum for 24 h at 65 °C. $CO_2$ is then pressurized with a Teledyne Isco 260D fully automated gas booster and used to charge the high-pressure cell. For each pressure point it takes about 45 min to reach equilibrium, and once temperature and pressure equilibrium is reached four different sets of measurements are made over a period of 10 min each. During the 10 min measurement periods, pressure, temperature and weight measurements are collected every 30 s along with the sinker weight measurements for in situ density values of the absorbate gas. Some pressure points might require repetition, depending on the experimental stability. Consequently, the total duration of each experimental sorption measurement is about 40 to 60 min. At the end of each pressure point measurement, the system goes to the next automatically. In this work, pressures up to 200 bar are used for maximum pressure, and at the end of each isotherm a hysteresis check is conducted by collecting desorption data as the system is depressurized. The temperature of the high-pressure cell is controlled by an automated external constant-temperature circulator (Polyscience model 9512) using a platinum resistance thermometer (Jumo DMM 5017 Pt100) attached to the high-pressure cell body. The cell temperature is maintained within ±0.6 °C accuracy. The automatic gas dosing system is used to control the pressure inside the high-pressure cell. The pressure control unit is a combination of shut valves, a special proportional–integral–derivative control instrument and a precise pressure transducer, Paroscientific Digiquartz 745-3 K with an accuracy of 0.01%. (See Supplementary methods and Supplementary Figs. 17–22 for more details of the Rubotherm magnetic suspension sorption apparatus and adsorbate memory effect study.)

**Solvent swelling measurements.** Solvent-induced swelling of COPs was determined in millilitres per gram using hexane, methanol and chloroform. Before swelling experiments, COPs were dried for 6 h at 120 °C. Swelling experiments were carried out in triplicate to minimize errors. The COPs (0.1–0.5 g) were weighed into an empty vial and the solvent of interest (10 ml) was added. The polymers were soaked in the solvent for 24 h under a closed lid. After 24 h, the samples were filtered with filter paper and immediately transferred onto a weighing paper, and the mass of the polymer was measured. The amount of absorbed solvent was measured by subtracting the initial mass of the polymer from the total swelled mass (see Supplementary Figs. 32–35 for more details of the Rubotherm magnetic suspension sorption apparatus and adsorbate memory effect study).

## Data availability

The data that support the plots within this paper and other findings of this study are available from the corresponding author on reasonable request.

Received: 22 March 2018; Accepted: 30 May 2019;
Published online: 8 July 2019

## References

1. Kumar, K. V., Preuss, K., Titirici, M.-M. & Rodríguez-Reinoso, F. Nanoporous materials for the onboard storage of natural gas. *Chem. Rev.* **117**, 1796–1825 (2017).
2. Mason, J. A. et al. Methane storage in flexible metal–organic frameworks with intrinsic thermal management. *Nature* **527**, 357–361 (2015).
3. Peng, Y. et al. Methane storage in metal–organic frameworks: current records, surprise findings, and challenges. *J. Am. Chem. Soc.* **135**, 11887–11894 (2013).
4. Li, B., Wen, H.-M., Zhou, W., Xu, J. Q. & Chen, B. Porous metal-organic frameworks: promising materials for methane storage. *Chem* **1**, 557–580 (2016).
5. Deria, P. et al. Beyond post-synthesis modification: evolution of metal-organic frameworks via building block replacement. *Chem. Soc. Rev.* **43**, 5896–5912 (2014).
6. Guillerm, V. et al. A supermolecular building approach for the design and construction of metal-organic frameworks. *Chem. Soc. Rev.* **43**, 6141–6172 (2014).
7. Li, M., Li, D., O'Keeffe, M. & Yaghi, O. M. Topological analysis of metal–organic frameworks with polytopic linkers and/or multiple building units and the minimal transitivity principle. *Chem. Rev.* **114**, 1343–1370 (2014).
8. Krause, S. et al. A pressure-amplifying framework material with negative gas adsorption transitions. *Nature* **532**, 348–352 (2016).
9. Jung, J. Y. et al. Limitations and high pressure behavior of MOF-5 for $CO_2$ capture. *Phys. Chem. Chem. Phys.* **15**, 14319–14327 (2013).
10. Byun, J., Patel, H. A., Thirion, D. & Yavuz, C. T. Charge-specific size-dependent separation of water-soluble organic molecules by fluorinated nanoporous networks. *Nat. Commun.* **7**, 13377 (2016).
11. Patel, H. A. et al. High capacity carbon dioxide adsorption by inexpensive covalent organic polymers. *J. Mater. Chem.* **22**, 8431–8437 (2012).
12. Tian, T. et al. A sol–gel monolithic metal–organic framework with enhanced methane uptake. *Nat. Mater.* **17**, 174–179 (2018).
13. Chang, G. et al. A microporous metal-organic framework with polarized trifluoromethyl groups for high methane storage. *Chem. Commun.* **51**, 14789–14792 (2015).
14. Li, B. et al. A porous metal–organic framework with dynamic pyrimidine groups exhibiting record high methane storage working capacity. *J. Am. Chem. Soc.* **136**, 6207–6210 (2014).
15. Ma, S. et al. Metal-organic framework from an anthracene derivative containing nanoscopic cages exhibiting high methane uptake. *J. Am. Chem. Soc.* **130**, 1012–1016 (2008).
16. Eddaoudi, M. et al. Systematic design of pore size and functionality in isoreticular MOFs and their application in methane storage. *Science* **295**, 469–472 (2002).
17. Olah, G. A., Reddy, V. P. & Prakash, G. K. S. in *Kirk-Othmer Encyclopedia of Chemical Technology* 159–199 (Wiley, 2000).
18. Martin, C. F. et al. Hypercrosslinked organic polymer networks as potential adsorbents for pre-combustion $CO_2$ capture. *J. Mater. Chem.* **21**, 5475–5483 (2011).
19. Tan, L. et al. Hypercrosslinked porous polymer materials: design, synthesis, and applications. *Chem. Soc. Rev.* **46**, 3322–3356 (2017).
20. Li, B. et al. A new strategy to microporous polymers: knitting rigid aromatic building blocks by external cross-linker. *Macromolecules* **44**, 2410–2414 (2011).
21. Wang, S. et al. Layered microporous polymers by solvent knitting method. *Sci. Adv.* **3**, e1602610 (2017).
22. Li, L., Cai, K., Wang, P., Ren, H. & Zhu, G. Construction of sole benzene ring porous aromatic frameworks and their high adsorption properties. *ACS Appl. Mater. Interfaces* **7**, 201–208 (2015).
23. Msayib, K. J. & McKeown, N. B. Inexpensive polyphenylene network polymers with enhanced microporosity. *J. Mater. Chem. A* **4**, 10110–10113 (2016).
24. Jiang, J. et al. High methane storage working capacity in metal–organic frameworks with acrylate links. *J. Am. Chem. Soc.* **138**, 10244–10251 (2016).
25. Ullah, R. et al. Investigation of ester- and amide-linker-based porous organic polymers for carbon dioxide capture and separation at wide temperatures and pressures. *ACS Appl. Mater. Interfaces* **8**, 20772–20785 (2016).
26. Mason, J. A., Veenstra, M. & Long, J. R. Evaluating metal-organic frameworks for natural gas storage. *Chem. Sci.* **5**, 32–51 (2014).
27. Yuan, D., Lu, W., Zhao, D. & Zhou, H.-C. Highly stable porous polymer networks with exceptionally high gas-uptake capacities. *Adv. Mater.* **23**, 3723–3725 (2011).
28. Casco, M. E. et al. High-pressure methane storage in porous materials: are carbon materials in the pole position? *Chem. Mater.* **27**, 959–964 (2015).
29. Patel, H. A., Byun, J. & Yavuz, C. T. Carbon dioxide capture adsorbents: chemistry and methods. *ChemSusChem* **10**, 1303–1317 (2017).
30. Wu, K. et al. Methane storage in nanoporous material at supercritical temperature over a wide range of pressures. *Sci. Rep.* **6**, 33461 (2016).
31. Alezi, D. et al. MOF crystal chemistry paving the way to gas storage needs: aluminum-based soc-MOF for $CH_4$, $O_2$, and $CO_2$ storage. *J. Am. Chem. Soc.* **137**, 13308–13318 (2015).
32. Kong, G. Q. et al. Expanded organic building units for the construction of highly porous metal–organic frameworks. *Chem. Eur. J.* **19**, 14886–14894 (2013).
33. He, Y., Zhou, W., Yildirim, T. & Chen, B. A series of metal–organic frameworks with high methane uptake and an empirical equation for predicting methane storage capacity. *Energy Environ. Sci.* **6**, 2735–2744 (2013).
34. DeSantis, D. et al. Techno-economic analysis of metal–organic frameworks for hydrogen and natural gas storage. *Energy Fuels* **31**, 2024–2032 (2017).

## Acknowledgements

This work was supported by National Research Foundation of Korea (NRF) grants funded by the Korean government (Ministry of Science, ICT and Future Planning) (nos NRF-2016R1A2B4011027, NRF-2017M3A7B4042140 and NRF-2017M3A7B4042235).

## Author contributions

V.R. synthesized and characterized all the sorbents. D.T. helped in syntheses and analyses. R.U. and M.A. carried out high-pressure pure-gas uptake studies. V.R. and J.L. tested COP-150 in an actual cylinder. M.J. and H.O. collected cryogenic (111K) $CH_4$ isotherms. M.A. explained the high-pressure behaviour of the sorbents. C.T.Y. conceived the project and wrote the manuscript with contributions from all authors.

## Competing interests

KAIST has filed a provisional patent application (10-2019-0058296) related to the new flexible porous polymers reported in this manuscript.

## Additional information

**Supplementary information** is available for this paper at https://doi.org/10.1038/s41560-019-0427-x.

**Reprints and permissions information** is available at www.nature.com/reprints.

**Correspondence and requests for materials** should be addressed to M.A. or C.T.Y.

**Publisher's note:** Springer Nature remains neutral with regard to jurisdictional claims in published maps and institutional affiliations.